doi.org/10.36721/PJPS.2026.39.7.205.1

# TLR9 agonists alleviate diabetic condition by promoting the maturation of differentiated bone marrow mesenchymal stem cells in rats

**Chuan Liu[1], Huayong Zheng[1], Peng Lu[1], Jing Tian[2], Yenuan Hu[3], Li Yao[4]* and Tiansheng Sun[1]***

[1]Department of Orthopedic, The Forth Medical Center of Chinese PLA General Hospital, Beijing, 100037, China
[2]Department of Pediatrics, The Seventh Medical Center of Chinese PLA General Hospital, Beijing, 100700, China
[3]Department of Medical Service, The Seventh Medical Center of Chinese PLA General Hospital, Beijing, 100700, China
[4]Department of Urology, The Seventh Medical Center of Chinese PLA General Hospital, Beijing, 100700, China

**Abstract**: **Background**: Current diabetes therapies often fail to address the loss of insulin-producing β-cells. Bone marrow mesenchymal stem cells (BMSCs) can differentiate into insulin-producing cells (IPCs), but functional maturity remains limited. Toll-like receptor 9 (TLR9) agonists may enhance BMSC maturation. **Objectives**: To investigate the ability of TLR9 agonists to promote the maturation of BMSCs in diabetic rats. **Methods**: BMSCs were isolated from rat bone marrow and identified by trilineage differentiation tests and flow cytometry. BMSCs were then differentiated into IPCs and treated with different concentrations of TLR9 agonists. PCR detected transcriptional levels of pancreatic endocrine-related genes. Diabetic model in rats was established using streptozotocin. BMSCs were encapsulated in TheraCyte capsules and subcutaneously transplanted into diabetic rats. Intraperitoneal injection of TLR9 agonists was performed, with serum insulin, C-peptide and fasting blood glucose (FBG) levels monitored in the transplanted rats. The recovered BMSCs were further characterized by immunofluorescence staining after the rats were killed. **Results**: Differentiated BMSCs displayed characteristics of IPCs, such as the ability to secrete insulin and C-peptide in *vitro*. Further, when exposed to gradient concentrations of TLR9 agonists, differentiated MSCs exhibited enhanced expression of pancreatic-associated endocrine genes and transcription factor levels. *In vivo, differentiated BMSC transplantation combined with TLR9 agonist administration notably improved diabetic conditions, as evidenced by suppressed FBG levels and elevated serum insulin and* C-peptide levels, comparable to those in the normal group. However, withdrawal of TLR9 agonists attenuated the therapeutic effects. Finally, immunofluorescence staining confirmed that a TLR9 agonist promoted IPC maturation, as evidenced by co-expression of insulin and C-peptide *in vivo*. **Conclusion**: TLR9 agonists promote the differentiation and functional maturation of BMSCs into IPCs, thereby improving metabolic parameters in diabetic rats. This "stem cell-immunomodulator" strategy provides a foundation for developing functional β-cell replacement therapies.

**Keywords**: BMSCs; Diabetes; IPCs; TLR9 agonists

*Submitted on 26-03-2025 – Revised on 28-02-2026 – Accepted on 04-03-2026*

## INTRODUCTION

Diabetes mellitus (DM) is one of the major health burdens facing the 21st century with increasing prevalence, characterized by multi-organ complications that account for the primary disability and mortality (Russo *et al*., 2023; Dilworth *et al*., 2024). For instance, long-term DM leads to nephropathy and cardiovascular injury, which ultimately severely limit patients' lives and increase mortality (Bjornstad *et al*., 2021; Chan and Chan, 2022; Mori *et al*., 2026; Wang *et al*., 2025; Wang *et al*., 2022). Therefore, it is urgent to develop novel strategies to improve upon current diabetes management options.

Bone marrow mesenchymal stromal cells (BMSCs) are a heterogeneous population of stem cells with multidirectional differentiation potential, which can inhibit apoptosis, promote angiogenesis and have been widely applied in various diseases (Wang *et al*., 2024; Shao *et al*., 2023; Saccu *et al*., 2022). BMSCs can suppress oxidative stress and the inflammatory response, thereby protecting against DM-related injury (Li *et al*., 2021; Ebrahim *et al*., 2022; Utami *et al*., 2023). In addition to their immunomodulatory effects, BMSCs are more desirable for differentiating into terminal cells to repair tissue and address functional disorders. Recent evidence suggests that BMSCs can differentiate into insulin-producing cells (IPCs) and holds promising potential for insulin production to ameliorate DM (Dai and Wang, 2025; Wang *et al*., 2021). However, the uncertain and uncontrollable terminal differentiation of BMSCs *in vivo* seriously limits this possibility. Hence, it is vital to identify effective drugs to promote BMSC maturation. Studies (Khokhani *et al*., 2025; Han *et al*., 2022) reported that Toll-like receptor 9 (TLR9) agonists can enhance BMSC maturation for osteoblast differentiation in vitro, thereby promoting callus formation

**Corresponding author:* e-mail: naijimi7p0@126.com; 806864769@qq.com

and bridging ring formation at fracture sites in rats and enhancing early bone repair after fracture. However, the role of TLR9 agonists for BMSCs differentiation and maturation into IPCs remains poorly understood. Therefore, this study aims to explore a novel combined strategy to enhance the efficacy of stem cell therapy for diabetes, thereby providing a reference for future translational research.

## MATERIALS AND METHODS

The abbreviations are shown in table 1. The experimental principle is illustrated in Fig. 1.

### *Animals*

Sprague-Dawley (SD) rats were from Shanghai Jiake Biotechnology Co., Ltd. (China) and were maintained at the Animal Laboratory Center of Anhui Medical University.

### *Isolation, culture and identification of rat BMSCs*

Isolation and Culture: Sprague-Dawley (SD) rats aged 6-8 weeks were euthanized by cervical dislocation. Under sterile conditions, the femurs and tibias were isolated. The bone marrow cavities were flushed with α-MEM medium supplemented with 10% fetal bovine serum (FBS). The cell suspension was seeded into culture flasks and incubated at 37°C in a humidified atmosphere containing 5% $CO_2$. The first medium change was performed after 72 hours to remove non-adherent cells, followed by medium changes every 3 days. When the cells reached 80%-90% confluence, they were passaged using 0.25% trypsin. Cells from passages 3-5 were used for subsequent experiments (Luo *et al*., 2022).

Analysis of Surface Markers by Flow Cytometry: Third-passage BMSCs were trypsinized and resuspended to form a single-cell suspension. The cells were incubated separately with the following fluorescently labeled antibodies at 4°C in the dark for 30 minutes: Positive markers: CD29, CD44, CD106; Negative markers: CD34, CD14, CD45 (all purchased from Nantong Yishi Biotechnology Co., Ltd., China). Isotype-matched antibodies served as controls. Analysis was performed using a flow cytometer and data were processed with CellQuest software. The identification criteria were: expression rate of positive markers >95% and expression rate of negative markers <5%.

### *Identification of Tri-differentiation*

Adipogenic differentiation: Cells were cultured in adipogenic induction medium (1μM dexamethasone, 0.5 mM IBMX, 10μM insulin, 200μM indomethacin) for 21 days and lipid droplets were visualized by Oil Red O staining.

Osteogenic differentiation: Cells were cultured in osteogenic induction medium (0.1μM dexamethasone, 10 mM β-glycerophosphate, 50μM ascorbic acid) for 28 days and calcium nodules were observed by Alizarin Red staining (Zhang *et al*., 2026).

Chondrogenic differentiation: $2\times10^5$ cells were centrifuged to form micromass pellets and cultured in chondrogenic induction medium (containing 1% ITS, 50 μM ascorbic acid, 0.1 μM dexamethasone, 10 ng/mL TGF-$\beta_3$) for 21 days and cartilage matrix was observed by Alcian Blue staining.

### *Differentiation procedures of rat BMSCs to IPCs*

Cells were cultured in serum-free low-sugar DMEM supplemented with 55 nm trichostatin A (TSA, Lihan biotech co., ltd., China) for 3 days. Then, the cells were cultured in high-sugar (25 mM) medium containing DMEM: DMEM/F12 (Nantong Yishi Biotech Co., Ltd., China) at a 1:1 ratio for 7 days. Exchange medium every 2 days with 10 nm glucagon-like peptide-1 (GLP-1, Xian Ding Biotechnology Co., Ltd., China) and 10 nm nicotinamide (Xian Ding Biotechnology Co., Ltd., China) in subsequent culture.

### *Characterization of BMSCs after differentiation*

*Immune markers*

Rat BMSCs (passages 3–5) were cultured in α-MEM medium supplemented with 10% fetal bovine serum (FBS, Cat. #F1234, Gibco) at 37°C under 5% $CO_2$. When the cells reached approximately 90% confluency, the culture medium was replaced with differentiation medium. For cell immunostaining, anti-insulin antibody (1:200, Verunselun Biologic Reagent Co., Ltd., China) and anti-C-peptide antibody (1:100, Chengdu Smart Biotech Co., Ltd., China) were used. Subsequently, Alexa Fluor 488-labeled anti-rat immunoglobulin G (IgG, Verunselun Bio Reagent Co., Ltd., China) and Alexa Fluor 555-labeled anti-rabbit IgG (Verunselun Bio Reagent Co., Ltd., China) were applied, and the staining intensity was analyzed by flow cytometry.

### *Immunocytochemical analysis*

Cells after four-stage induction differentiation (IPCs) and undifferentiated BMSCs (control group) were seeded into confocal dishes. After reaching confluence, the cells were fixed with 4% paraformaldehyde at room temperature for 15 minutes, followed by three washes with PBS. Blocking was performed using a blocking buffer containing 5% goat serum and 0.3% Triton X-100 at room temperature for 1 hour. Subsequently, primary antibodies were added: rabbit anti-rat insulin polyclonal antibody (diluted 1:200) and mouse anti-rat C-peptide monoclonal antibody (diluted 1:100) and the mixture was incubated overnight at 4°C.

The next day, after washing with PBS, corresponding fluorescent secondary antibodies were added: Alexa Fluor 488-labeled goat anti-rabbit IgG (1:500, green fluorescence) and Alexa Fluor 555-labeled goat anti-mouse IgG (1:500, red fluorescence), followed by incubation at room temperature in the dark for 2 hours. Finally, cell nuclei were counterstained with DAPI (1 μg/mL) for 5 minutes.

**Table 1**: Abbreviations list

| Abbreviation | Full name |
|---|---|
| TLR9 | Toll-like receptor 9 |
| DM | Diabetes mellitus |
| BMSCs | Bone marrow mesenchymal stem cells |
| IPCs | Insulin-producing cells |
| STZ | Streptozotocin |
| FBG | Fasting blood glucose |
| ELISA | Enzyme-linked immunosorbent assay |
| PCR | Polymerase chain reaction |
| qRT-PCR/qPCR | Quantitative real-time polymerase chain reaction |
| DMSO | Dimethyl sulfoxide |
| SD | Sprague Dawley (rat) |
| α-MEM | Alpha Minimum Essential Medium |
| ITS | Insulin-Transferrin-Selenium |
| GLP-1 | Glucagon-like peptide-1 |
| TSA | Trichostatin A |
| PBS | Phosphate-buffered saline |
| SEM | Standard error of the mean |
| ANOVA | Analysis of variance |
| PDX1 | Pancreatic and duodenal homeobox 1 |
| NeuroD1 | Neurogenic differentiation 1 |
| GCG | Glucagon |
| SST | Somatostatin |
| Ngn3 | Neurogenin 3 |
| Pax4 | Paired box 4 |
| GAPDH | Glyceraldehyde-3-phosphate dehydrogenase |
| NF-KB | Nuclear factor kappa B |
| NLRP3 | NLR family pyrin domain containing 3 |
| MAPK | Mitogen-activated protein kinase |
| IRF7 | Interferon regulatory factor 7 |
| JAK-STAT | Janus kinase-signal transducer and activator of transcription |
| MyD88 | Myeloid differentiation primary response 88 |

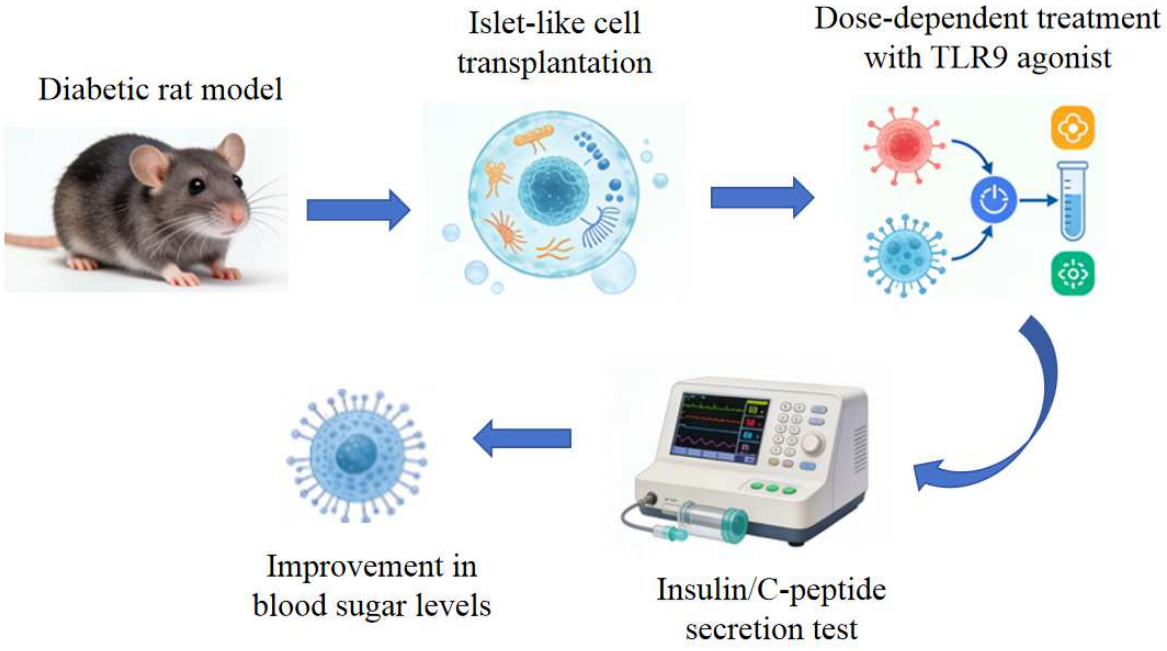


**Fig. 1**: Experimental flowchart

**Table 2**: PCR Primer sequences used

| Gene | Forward primer (5, -3,) | Reverse primer (5, -3,) |
|---|---|---|
| INS | CACCTTTGTGGTCCTCACCT | GACGGGACTTGGGTGTGTAG |
| GCG | CATTCACAGGGCACATTCAC | CGGTTCCTCTTGGTGTTCAT |
| PDX1 | TGCCACCATGAATAGTGAGG | CAGGGGGATTAGCACTGAAC |
| SST | GCTACTGGAGTCGTCTCTGC | CTCAGACAGCCGAGCTTGAG |
| Ngn3 | CAGCCTCATTGGAGGAGTTC | GGCCCTTCACAAGAAGTCTG |
| Pax4 | ATGGCGCAGACAAGAGAAGT | GGACTGCTGTGCAGAGATGA |
| Neurod1 | AGCCCCCTAACTGATTGCAC | TCGGTGGATGGTTCGTGTT |
| GAPDH | TGCCACTCAGAAGACTGTGG | TGGTACATGACAAGGTGCGG |

All staining steps were performed under light-protected conditions. Image Acquisition and Analysis: Stained samples were imaged using a Leica TCS SP8 laser scanning confocal microscope. For quantitative analysis, at least six non-overlapping fields (magnification ×100) were randomly selected per group and analyzed in a blinded manner using ImageJ software (version 1.53). Quantitative metrics included: Percentage of positive cells: The total number of DAPI-positive nuclei and the number of cells with colocalized insulin or C-peptide fluorescent signals were counted. The percentages of insulin-positive and C-peptide-positive cells were calculated separately. Mean fluorescence intensity (MFI): The average fluorescence intensity within the region of each positive cell was measured, with background fluorescence subtracted. Colocalization analysis: The Pearson correlation coefficient between insulin and C-peptide fluorescent signals was calculated using the "Colocalization Finder" plugin in ImageJ to assess the degree of co-expression of the two hormones at the subcellular level.

***In vitro release of insulin and c peptides***

Supernatant was collected after 24 h of culture. The rat insulin and c-peptide-linked immunosorbent assay (ELISA) kit (Chengdu Smart Biotechnology Co., Ltd., China) was used to determine insulin and c-peptide levels in rats.

***qRT-PCR assay***

Employed TLR9 agonist (SD-101, Shenzhen Xinbo Sheng Biotech Co., Ltd) (1 μM, 2.5 μM, 5 μM) to pretreat BMSCs for 24 h with DMSO as control. Total RNA extraction and quality control: Total RNA was extracted using TRIzol® Reagent according to the manufacturer's instructions. Extract total RNA from BMSCs from different treatment groups. Use the NanoDrop™ 2000 ultramicro spectrophotometer (Thermo Fisher Scientific) to measure RNA concentration and purity. Ensure that the A260/A280 ratio of all samples is between 1.8-2.0 and the A260/A230 ratio is greater than 2.0. cDNA synthesis: Use PrimeScript™ RT reagent Kit with gDNA Eraser (Takara Bio) for reverse transcription reaction. Take 1 μg of total RNA, first treated with gDNA Eraser to remove genomic DNA contamination and then perform reverse transcription reaction using random hexamer primers and/or Oligo(dT) primers. The reaction system and procedure strictly follow the instructions of the reagent kit. The obtained cDNA is stored at -20°C for future use. Real-time fluorescence quantitative PCR: Use TB Green® Premix Ex Taq™ II (Takara Bio), on the QuantStudio 5 Real-Time PCR System (Applied Biosystems). The reaction system is 20 μL: cDNA template, 2 μL; upstream and downstream primers (10 μM), each 0.4 μL; pre-mix enzyme, 10 μL; supplemented with nuclease-free water. The primer sequences are shown in table 2. The reaction program is: 95°C pre-denaturation for 30 seconds; then 40 cycles (95°C denaturation for 5 seconds, 60°C annealing/extension for 30 seconds). Each sample is set with 3 technical replicates and a no-template control (NOC) and a no-reverse transcription control (NTC) are included to exclude contamination and genomic DNA interference. Data analysis: Calculate the relative expression of the target gene using the $2^{-\Delta\Delta Ct}$ method. Use the Gapdh gene as the internal reference for normalization (Duan *et al*., 2023). The data is presented as mean ± standard error. It should be noted that to determine the effective concentration range of the TLR9 agonist for the differentiation of BMSC-IPCs and to evaluate its dose-dependent effect, we set gradient concentrations (1, 2.5, 5 μM) of SD-101 for treatment during the *in vitro* differentiation stage. The aim is to identify the optimal concentration that maximizes the expression of functional genes of IPCs; and to observe whether this effect is dose-dependent, thereby providing support for its specific action; and to provide direct experimental evidence for the selection of the dose for subsequent *in vivo* treatment.

***TheraCyte™ encapsulation method***

The differentiated BMSC-IPCs were encapsulated using the Immune Isolation Device (TheraCyte™ capsule, Chengdu Smart Biotechnology Co., Ltd., China) (Waris *et al*., 2026). In a laminar flow hood, the sterile capsules were balanced with sterile PBS for 30 minutes, then transferred to α-MEM medium containing 10% autologous rat serum and pre-treated at 37°C for 2 hours to enhance biocompatibility. The differentiated cells were collected and gently resuspended with pre-cooled matrix gel (Corning Matrigel® Growth Factor Reduced, diluted 1:1 with serum-free medium) to prepare a cell suspension with a density of $1\times10^8$ cells/mL (operated on ice). Using sterile micropipettes, 50 μL of the cell suspension (containing

$5\times10^6$ cells) was slowly injected into the capsule cell chamber, avoiding bubble formation. After injection, the chamber was left to stand at room temperature for 15 minutes to allow the matrix gel to slightly polymerize and then the sealing clamp and 6-0 polypropylene suture provided with the equipment were used to firmly ligate the filling port. The encapsulated capsules were cultured in complete medium for a short period (37°C, 2 hours) before transplantation.

***Establishment of diabetic model and cell transplantation and TLR9 agonist management in rats***

Rats were free to feed and drink water and the animal room maintained a temperature of 20-25ºC and provided a certain amount of light (Wen *et al*., 2024). Three days later, rats were randomly assigned to an experimental group and a control group. All rats start fasting 12 hours before the start of the experiment, with free access to water. Fasting time can be extended to 18 hours if necessary, but not more than 24 hours. The STZ solution was protected from light using aluminum foil and stored in ice water. The STZ solution was injected within 30 minutes. The weight of rats was measured after an intraperitoneal injection of 45 mg/kg. The control group received citric acid-sodium citrate buffer solution. Blood glucose determination: blood glucose was measured and recorded by intraperitoneal injection at 48 and 72 hours in STZ-treated rats. A blood glucose level above 16.8 mmol/L for 3 consecutive days indicates that the model is successful.

10 diabetic rats were treated as untreated diabetic controls and injected daily with DMSO (vehicle control); the remaining 20 diabetic rats were transplanted with 5 × 10^6 BMSCs. The cells were loaded into a package device (TheraCyte™ capsule, Chengdu Smart Biotechnology Co., Ltd., China) and transplanted under the back skin of rats. After the rats were anesthetized with 2% isoflurane, a skin incision approximately 1 cm in length was made in the dorsal scapular area. The encapsulated cell capsules were implanted into the subcutaneous fascia layer and fixed to the surrounding tissues with 6-0 absorbable sutures. The skin incision was closed with surgical clips and postoperative subcutaneous injection of analgesic drug (butorphanol, 0.1 mg/kg) was performed. After 24 h of transplantation, 10 rats were intraperitoneally injected with TLR9 agonists (50 mg/kg) and the other 10 rats were injected with 25 mg/kg TLR9 agonists once a day for 6 weeks, or were discontinued from TLR9 agonists instead of DMSO.

***Monitoring biochemical indicators***

6 weeks of monitoring for fasting blood glucose FBG, insulin and c peptide were performed monthly. glucose tolerance curves were performed at 24 weeks. In the end, animals were sacrificed and BMSCs cells encapsulated in TheraCyte™ capsules were collected for immunohistochemical analysis.

***Immunofluorescence analysis***

At the end of the experiment, the rats were sacrificed and the TheraCyte™ capsules were recovered for paraffin embedding and sectioning (3 μm). The sections were subjected to antigen retrieval and then incubated overnight at 4°C with insulin (1:200) and C-peptide (1:100) primary antibodies, followed by 2 hours at room temperature with the corresponding fluorescent secondary antibodies (Alexa Fluor 488/555). DAPI was used for nuclear staining. After image acquisition, a researcher unaware of the experimental groups used ImageJ (version 1.53) for analysis. The proportion of positive cells: At least 5 animals in each group were analyzed and 3 non-overlapping fields of view (×100 magnification) were randomly selected from each animal's capsule section. The total number of DAPI-positive cell nuclei in each field was counted, as well as the number of cells where insulin and C-peptide signals co-localized with the cell nuclei. The proportion of insulin-positive cells = (number of insulin-positive cells / total number of cell nuclei) × 100%; The calculation formula for C-peptide-positive cell proportion is the same as above; The proportion of double-positive cells = (number of cells with both insulin and C-peptide signals positive / total number of cell nuclei) × 100%. Average fluorescence intensity: Using ImageJ software, after identifying the positive cell area, the average fluorescence intensity of the insulin and C-peptide channels within this area was measured and the background fluorescence in the same field without cells was subtracted. Co-localization analysis: Using the "Colocalization" plugin in ImageJ, the Pearson correlation coefficient between insulin and C-peptide fluorescence signals in the same field was calculated to quantify their subcellular co-expression.

***Quantification and blind analysis of immunofluorescence images***

All the analysis of the immunofluorescence images was conducted in a blinded manner. The image files were randomly renamed and a researcher unaware of the experimental groups used ImageJ (version 1.53, NIH) to analyze them. For the transplanted capsule sections, at least 5 non-overlapping fields of view were randomly selected. The total number of DAPI-positive cell nuclei and the number of cells with co-localization of insulin (or C-peptide) signals and cell nuclei were counted and the percentage of positive cells was calculated. At the same time, the average fluorescence intensity of the positive signal area in each field of view (after background subtraction) was measured. After the final data was unblinded, statistical comparisons between groups were performed.

***Sample size calculation***

The sample size was calculated using G*Power 3.1.9.2. The sample size calculation was based on the difference in fasting blood glucose between diabetic model rats and

diabetic rats that had undergone preliminary treatment. A one-way repeated measures analysis of variance was used. Based on the results of the previous pre-experiment, an effect size of 2.54, a significance level of 0.05 and a power of 0.95 were adopted. After calculation, at least 6 rats were required per group. Considering experimental losses, 10 rats were included per group, yielding a total sample size of 40.

***Quality control***

All chemical reagents used in this study were of analytical-grade or cell culture-grade purity. All key reagents and consumables were sourced from the same batch and used in the same series of experiments to reduce variation. Antibodies and ELISA kits were validated before use to ensure specificity. All subjective evaluations, such as histological image analysis and cell counting were conducted in a blinded manner. Instruments and equipment were calibrated according to standard procedures before use.

***Statistical analysis***

Results are expressed as mean ± standard error of the mean (SEM). All continuous data were first assessed for normality using the Shapiro-Wilk test. For data that followed a normal distribution, one-way analysis of variance (ANOVA) was used to compare more than two groups, followed by Tukey's post hoc test if the main effect was significant; comparisons between two groups were performed using an unpaired Student's t-test. For data that did not follow a normal distribution, the Kruskal-Wallis test was used for comparisons among more than two groups, followed by Dunn's post hoc test if the main effect was significant; comparisons between two groups were performed using the Mann-Whitney U test. A p-value of less than 0.05 ($p < 0.05$) was considered statistically significant.

## RESULTS

***Identification and analysis of BMSCs***

BMSCs adhered to plastic and appeared predominantly spindle-shaped, with visible cytoplasmic processes and clearly defined nuclei. Flow cytometry analysis revealed that the third-generation cells highly expressed the mesenchymal stem cell positive markers CD29 (99.2%), CD44 (98.5%) and CD106 (97.8%), while they almost did not express the negative markers for the hematopoietic system and monocytes, such as CD34 (0.032%), CD14 (0.33%) and CD45 (0.032%).Oil Red O staining (bright red indicates lipid droplets) and Alizarin Red staining (bright red indicates calcium nodules) confirmed adipogenic and osteogenic differentiation capacity, respectively. Cartilage potential has been also identified by Alcian blue staining (Fig. 2, 3).Quantitative analysis showed that after induction, the area of oil red O staining positive regions accounted for (42.7 ± 6.3)% of the field area, which was significantly higher than that of the uninduced control group ((2.1 ± 1.5)%, $P< 0.001$) (Fig. 3D). The number of mineralized nodules shown by alizarin red staining (28.5 ± 4.8 per field vs. control group 1.2 ± 1.0 per field, $P< 0.001$) (Fig. 3E) and the absorbance of alizarin blue staining (0.85 ± 0.12 A.U. vs. control group 0.15 ± 0.05 A.U., $P< 0.001$) (Fig. 3F) were all significantly increased. These results are consistent with the ISCT definition of BMSCs, confirming that the cells we used are rat BMSCs.

***The differentiation of BMSCs into IPCs and their in vitro functions***

After four-stage induction differentiation, BMSCs successfully differentiated into IPCs. Immunofluorescence staining showed that the differentiated cells simultaneously expressed insulin (green) and C-peptide (red) and both were co-localized in the cytoplasm (yellow) (Figs. 4A–C). Quantitative analysis indicated that the proportion of insulin-positive cells was (65.2 ± 8.4)%, the proportion of C-peptide-positive cells was (61.8 ± 7.9)% and the average fluorescence intensities were (3200 ± 450) A.U. and (2850 ± 400) A.U., respectively, which were significantly higher than those of the undifferentiated control group ($P < 0.001$) (Figs. 4D, E). Pearson's colocalization coefficient for insulin and C-peptide signals was 0.88 ± 0.05 (Fig. 4F). Under glucose stimulation, the secretion of insulin and C-peptide by the differentiated cells significantly increased with the increase in glucose concentration (Figs. 5A, B).

***The TLR9 agonist promotes gene expression in BMSC-IPCs.***

Differentiated BMSCs-IPCs were treated with TLR9 agonist SD-101 at gradient concentrations (1, 2.5, 5 μM). The qRT-PCR results showed that the TLR9 agonist significantly upregulated multiple pancreatic endocrine-related genes in a dose-dependent manner, including INS, GCG, PDX1, SST, Ngn3, Pax4 and NeuroD1 (Fig. 6).

***TLR9 agonist combined with BMSCs transplantation improves metabolic indicators in diabetic rats***

After successfully establishing the STZ-induced diabetic rat model, differentiated BMSCs-IPCs were encapsulated in TheraCyte capsules and transplanted subcutaneously into the rats. After the operation, the TLR9 agonist (25mg/kg or 50mg/kg) was continuously injected intraperitoneally for 6 weeks. The results showed that, compared with the diabetic control group, BMSC transplantation combined with a TLR9 agonist significantly reduced fasting blood glucose levels (Fig. 7) and the high-dose group (50 mg/kg) had a more significant hypoglycemic effect. The serum insulin and C-peptide levels of the treatment group rats significantly increased (Fig. 8, 9), approaching those of the normal control group and the increase in the high-dose group was greater.

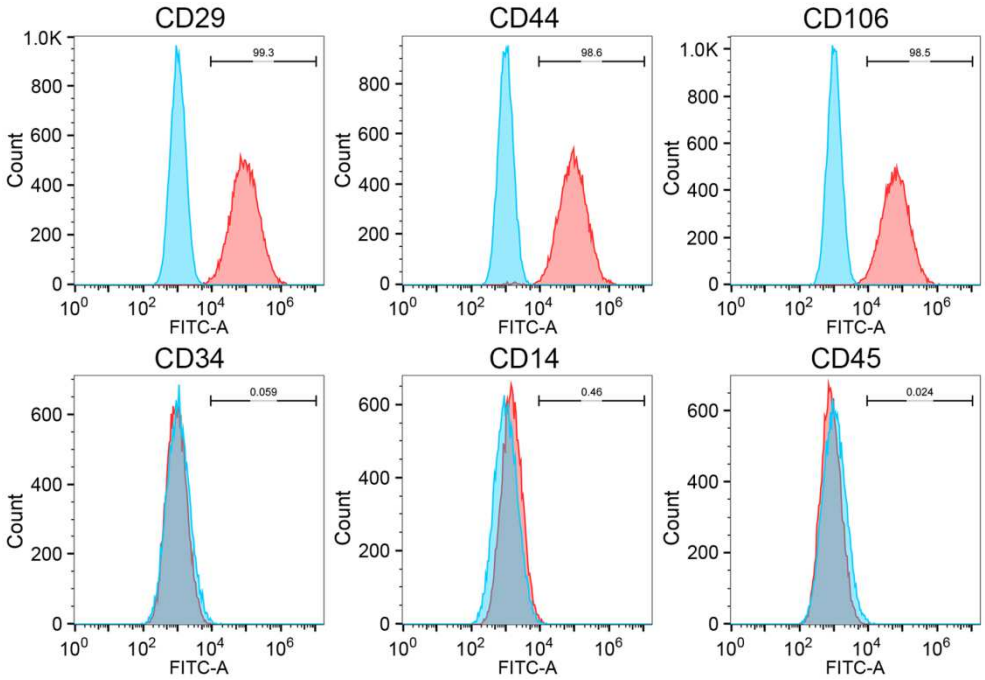


**Fig. 2**: Analysis of BMSCs surface marker levels by flow cytometry.
Note: The bar chart shows the average fluorescence intensity or positive percentage of the positive markers (CD29, CD44, CD106) and the negative markers (CD34, CD14, CD45). The data are from n = 3 independent cell isolation batches, and at least 10,000 cells were analyzed in each batch.

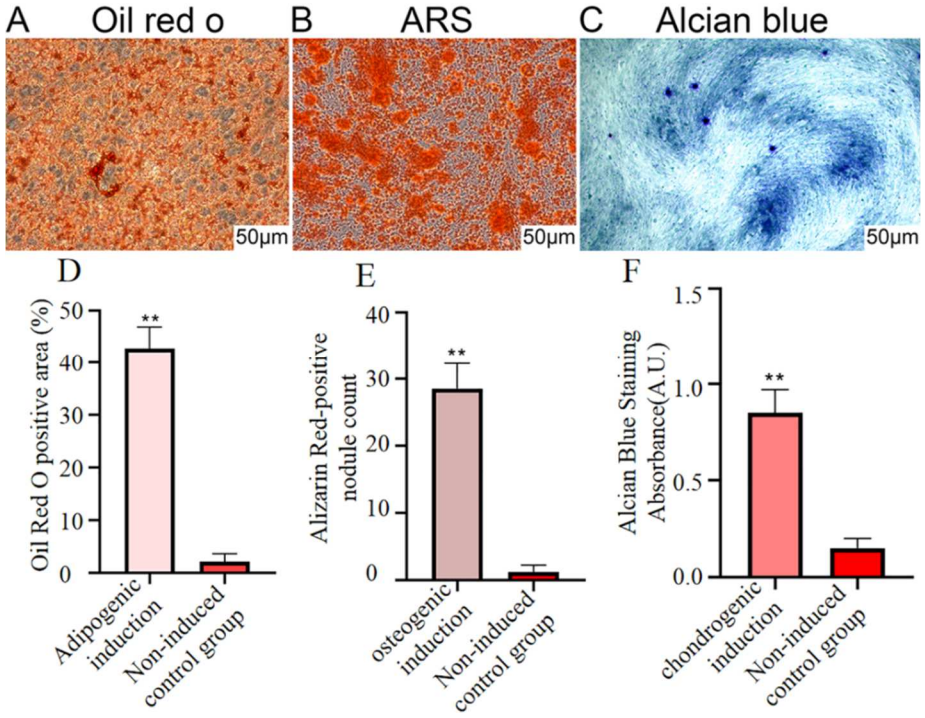


**Fig. 3**: Identification of differentiation potential of BMSCs in rats.
Oil red o staining for adipogenesis (original image x50); (B) Alizarin red staining for ossification (original image x50); And (C) Alcian blue for cartilage formation (original image x50); (D) Percentage of oil red O positive area; (E) Alizarin red-positive mineralized nodule counting; (F) Absorbance of Alcian blue staining (background subtracted). Note: Data are mean ± SD (n = 5 independent fields/group, with each group of cells derived from 3 independent culture batches); compared with the uninduced control group, **P < 0.001.

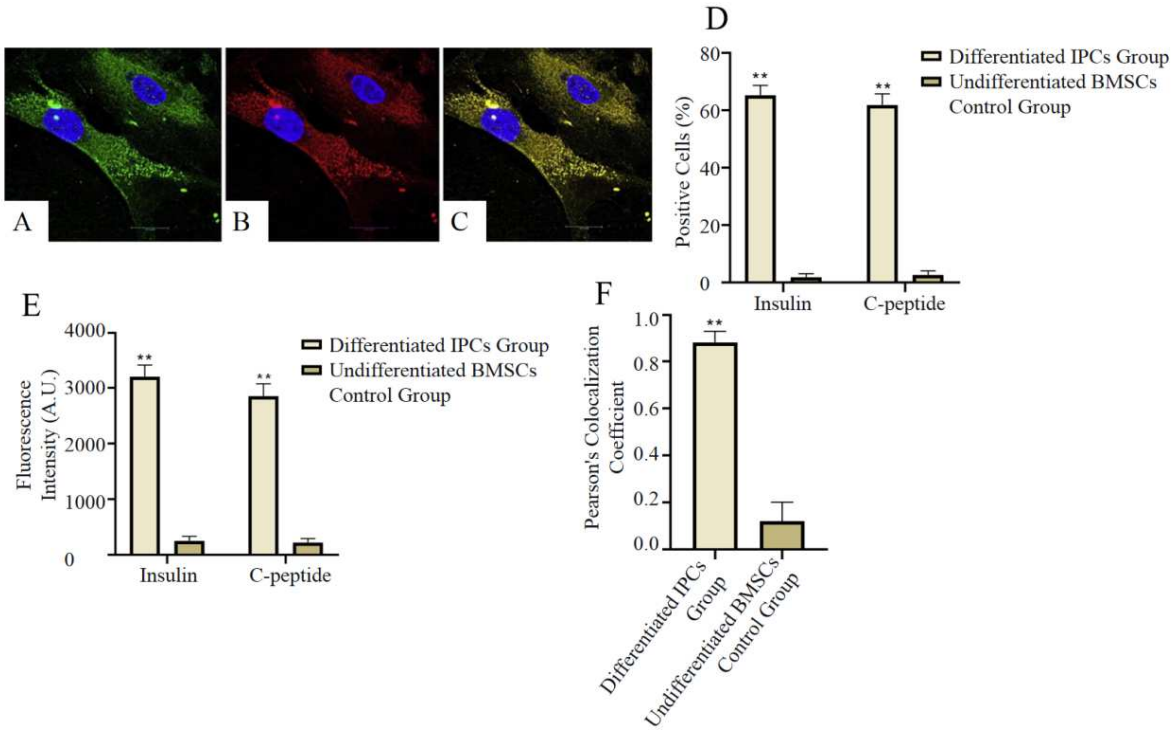


**Fig. 4**: Physiological characteristics of BMSCs-derived IPCs with differentiation by immunofluorescence analysis. Immunofluorescence staining for insulin (Green, original x100). (B) Immunofluorescence staining for C-peptide (Red, original image x100), (C) Merge showing co-localization of insulin and C-peptide in differentiated IPCs (Yellow, original image x100).Nuclei are counterstained with DAPI (Blue)； (D) Percentage of insulin and C-peptide positive cells; (E) Average fluorescence intensity of insulin and C-peptide; (F) Pearson's co-localization coefficient of insulin and C-peptide signals. Note: The data are mean ± SD (n = 6 independent fields/group, from 3 independent differentiation experiments; undifferentiated BMSCs were used as the control); Compared with the control group, **P < 0.001.

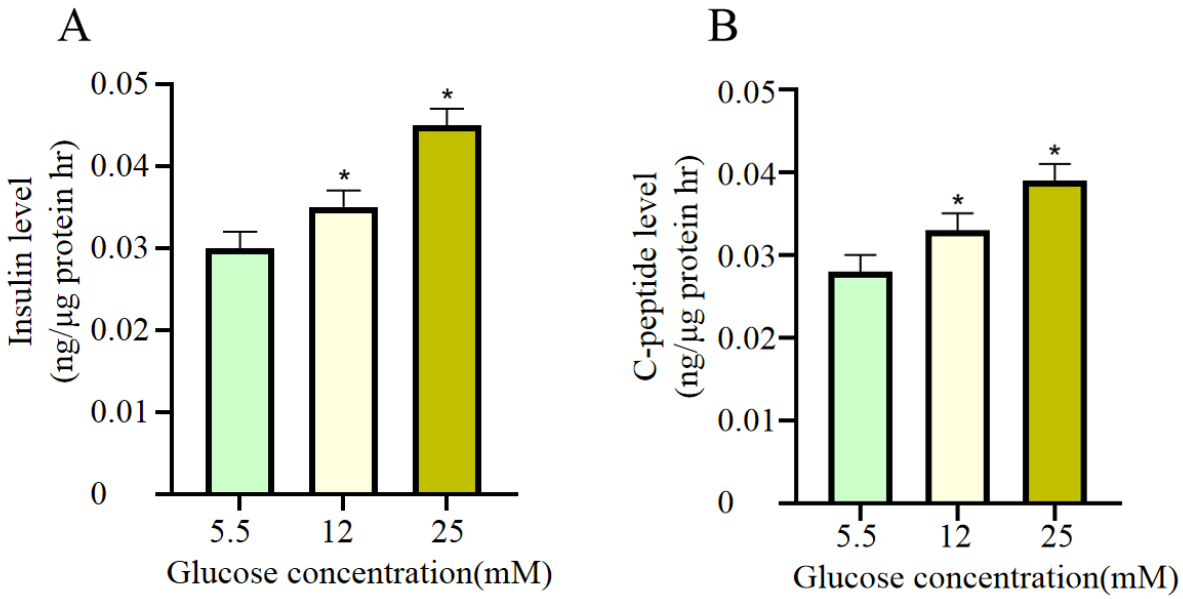


**Fig. 5**: Secretion of insulin and C-peptide after glucose treatment.
Insulin (A) and c peptide (B) secretion in differentiated cells at different glucose concentrations, * P<0.05.
Note: The data are presented as mean ± SEM (n = 4 independent differentiated samples, with 2 technical replicates for each sample).

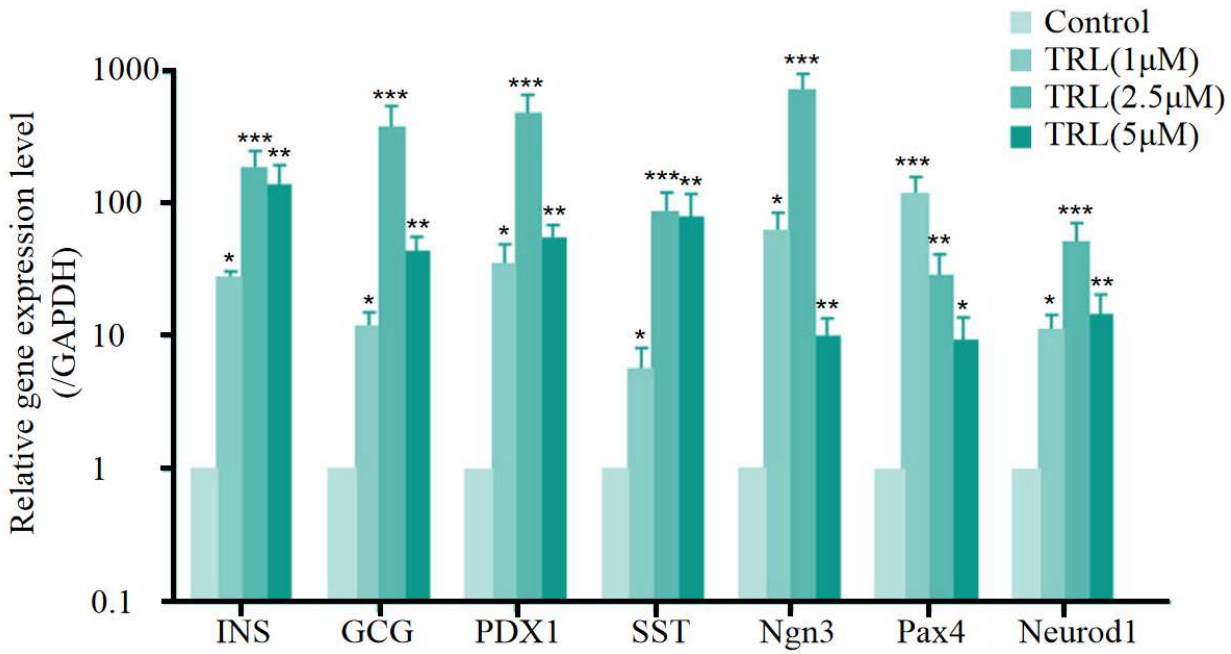


**Fig. 6**: Expression of diabetes-related genes in differentiated BMSCs treated with different concentrations of TLR9 agonists.

Note: After treating differentiated BMSCs with gradient concentrations of TLR9 agonist SD-101 (1, 2.5, 5 μM) for 24 hours, the mRNA expression levels of pancreatic endocrine-related genes were detected by qRT-PCR. The data were normalized with Gapdh as the internal reference and based on the DMSO control group. The data are the mean ± SEM (n = 3 independent biological replicates, each replicate from different batches of cell isolation and differentiation). * P<0.05, ** P<0.01, *** P<0.001 vs. DMSO control group (one-way ANOVA, Dunnett's post-hoc test).

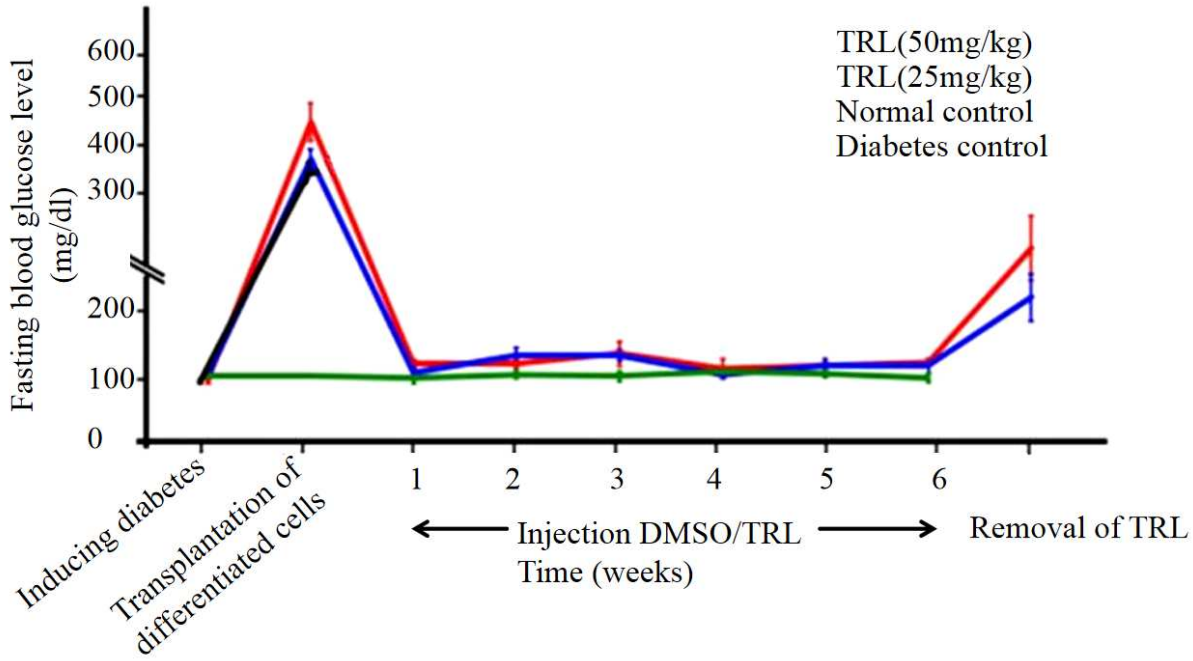


**Fig. 7**: Changes of FBG level in four groups of rats.

Note: The trends of fasting blood glucose changes in the four groups of rats. Grouping: Diabetes control group (DM Control, n=10), BMSCs transplantation group (BMSCs Only, n=10), BMSCs + TLR9 (25 mg/kg) group (n=10), BMSCs + TLR9 (50 mg/kg) group (n=10).

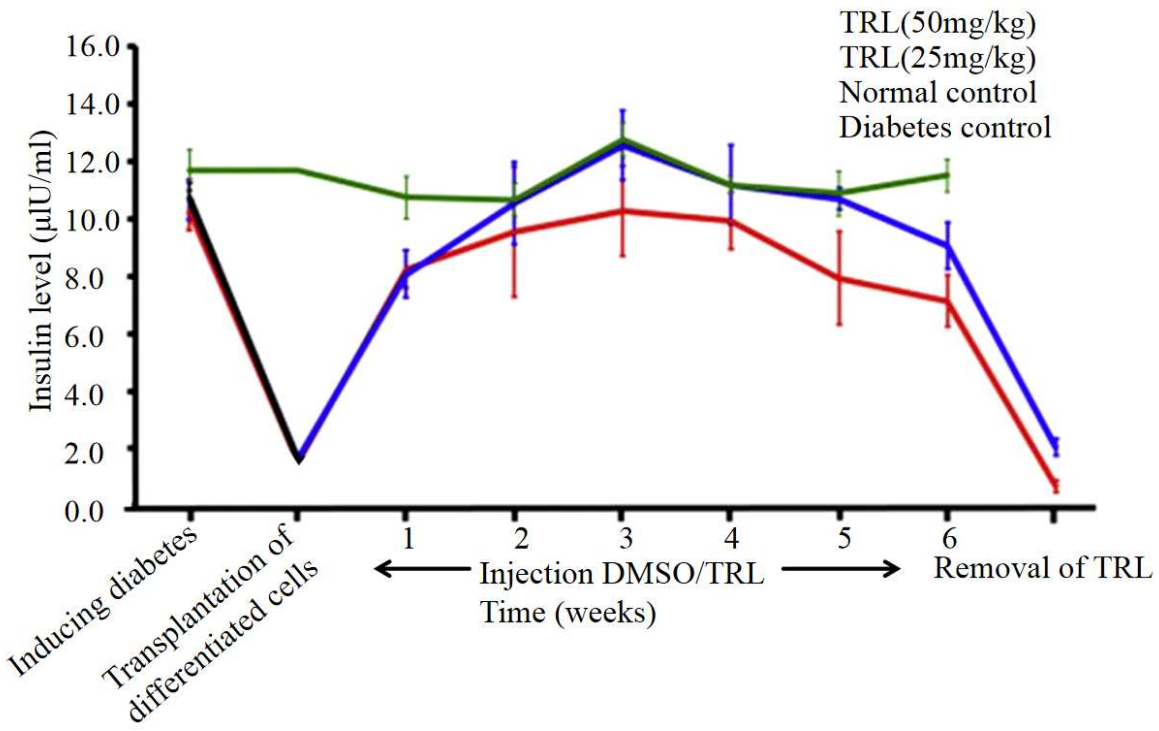


**Fig. 8**: Changes of serum insulin levels in four groups of rats.
Note: The trends of insulin changes in the four groups of rats. Grouping: Diabetes control group (DM Control, n=10), BMSCs transplantation group (BMSCs Only, n=10), BMSCs + TLR9 (25 mg/kg) group (n=10), BMSCs + TLR9 (50 mg/kg) group (n=10).

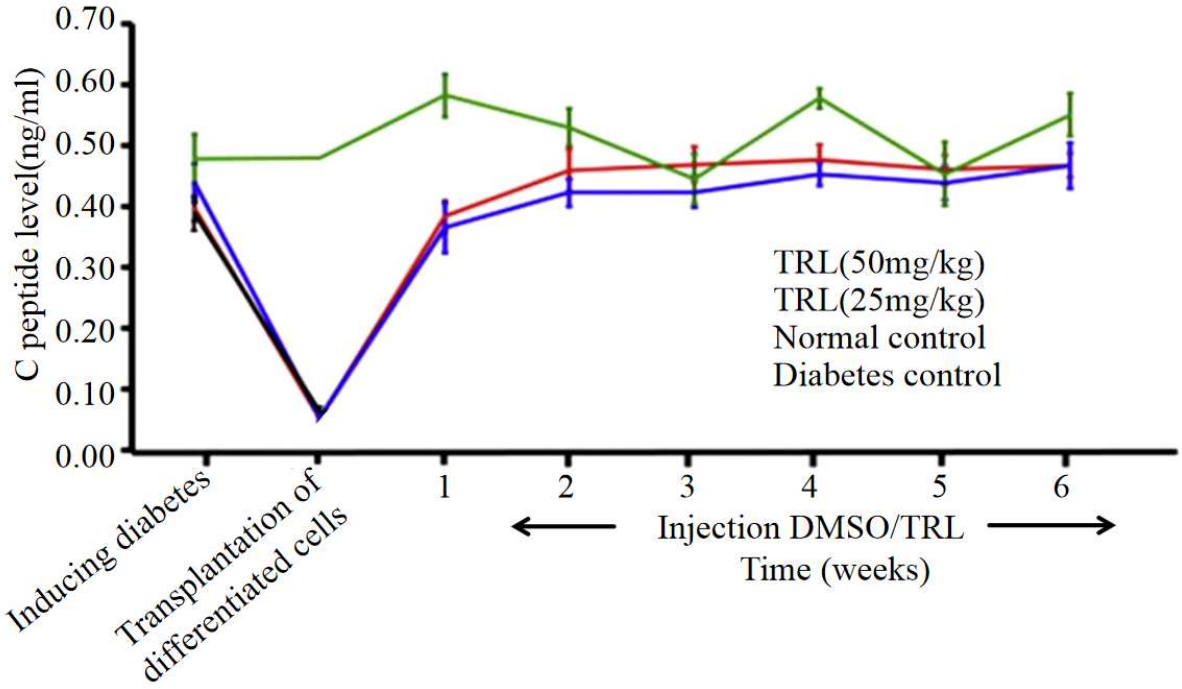


**Fig. 9**: Changes of serum c- peptide levels in four groups of rats.
Note: The changes in C-peptide levels of the four groups of rats. Grouping: Diabetes control group (DM Control, n=10), BMSCs transplantation group (BMSCs Only, n=10), BMSCs + TLR9 (25 mg/kg) group (n=10), BMSCs + TLR9 (50 mg/kg) group (n=10).

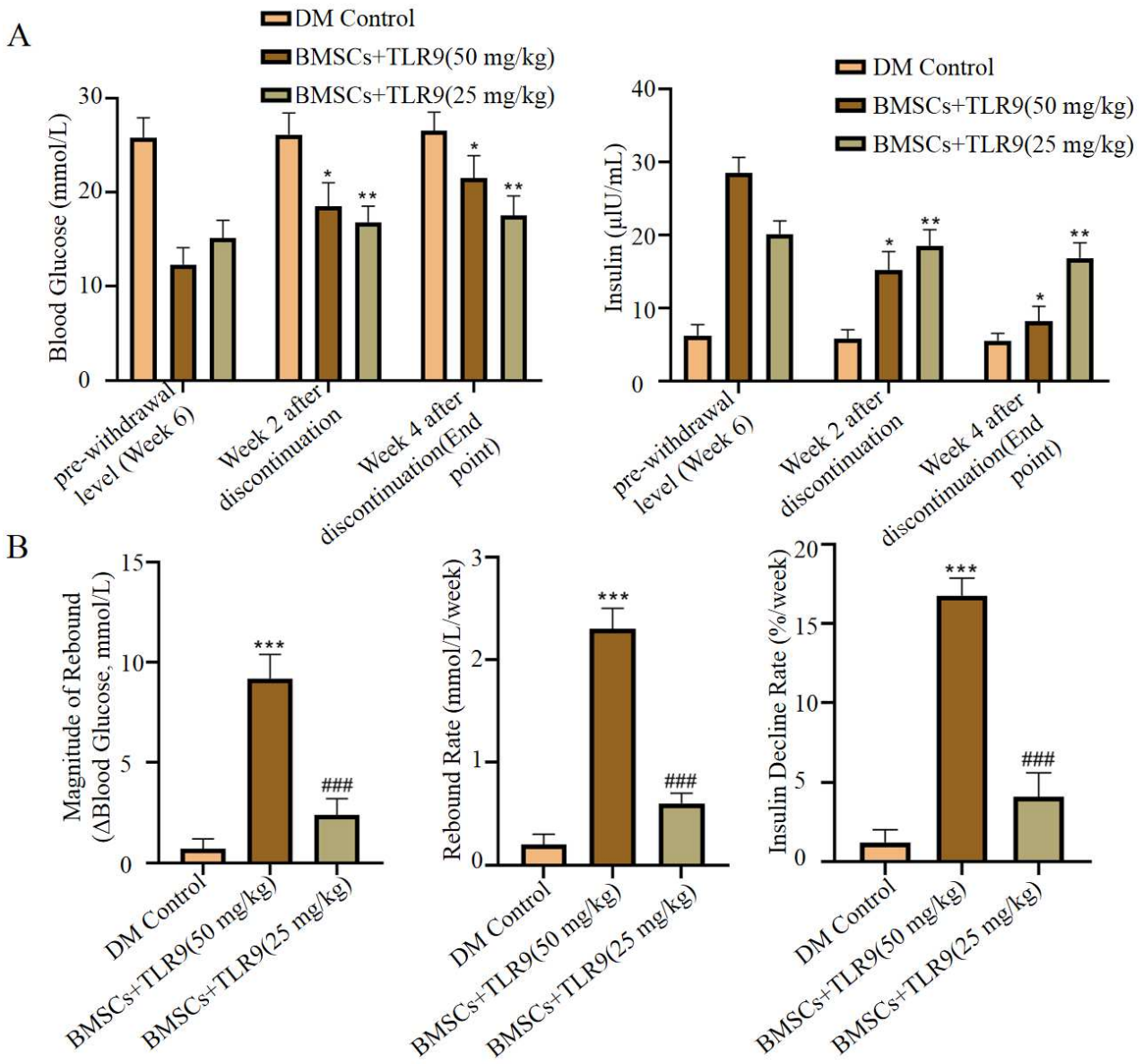


**Fig. 10**: Quantitative analysis of therapeutic rebound after drug withdrawal.
(A) Quantitative analysis diagram of rebound dynamics. Diabetes control group (n=10), BMSCs + TLR9 (25 mg/kg) group (n=10), BMSCs + TLR9 (50 mg/kg) group (n=10). Data are mean ± SEM. *P < 0.05, **P < 0.01 compared with the withdrawal level before (Week 6). (B) Quantitative comparison diagram of rebound amplitude and rate. Diabetes control group (n=10), BMSCs + TLR9 (25 mg/kg) group (n=10), BMSCs + TLR9 (50 mg/kg) group (n=10). ### P < 0.001 compared with the DM Control group; ***P < 0.001 compared with the BMSCs + TLR9 (25 mg/kg) group.

After stopping the TLR9 agonist treatment, the fasting blood glucose, insulin and C-peptide levels of the high-dose group rapidly returned to levels close to those of the diabetic control group (Fig. 10), suggesting that the therapeutic effect depends on continuous agonist stimulation and cannot be maintained after discontinuation.

***Quantitative analysis of rebound effect after drug withdrawal***

Although continuous administration of TLR9 agonist can effectively control blood glucose, drug withdrawal caused a rapid and significant metabolic reversal (Fig. 10A). In the BMSCs + TLR9 (50 mg/kg) group, after drug withdrawal, the fasting blood glucose rebounded from the 12.3 ± 1.8 mmol/L at the time of withdrawal to 21.5 ± 2.4 mmol/L (an increase of 74.8%, $P < 0.001$), which was no longer different from the diabetic control group ($P > 0.05$). At the same time, the serum insulin decreased from 28.5 ± 3.1 μIU/mL to 8.2 ± 2.0 μIU/mL (a decrease of 71.2%, $P < 0.001$). The quantitative analysis of the rebound effect showed that the rebound amplitude (9.2 ± 1.2 mmol/L) and rebound rate (2.3 ± 0.3 mmol/L/week) of the high-dose

drug withdrawal group were significantly higher than those of the low-dose drug withdrawal group (amplitude: 2.4 ± 0.8 mmol/L; rate: 0.6 ± 0.2 mmol/L/week) and all continuous treatment groups (all comparisons $P < 0.001$) (Fig. 10B). Correspondingly, the insulin decline rate (-16.8 ± 2.1 %/week) of the high-dose drug withdrawal group was also significantly faster than that of the low-dose group (-4.1 ± 1.5 %/week, $P < 0.001$).

***Oral glucose tolerance test***

The BMSCs transplantation combined with TLR9 agonist treatment group showed lower blood glucose levels and higher insulin secretion than the diabetic control group, but their metabolic status still showed significant differences from the normal control group (Fig. 11).

***Immunofluorescence and histological studies***

After the experiment, the transplanted capsules were retrieved for immunofluorescence analysis. The results showed that the cells within the capsules still expressed insulin (green) and C-peptide (red) and both were co-expressed in the cytoplasm (Figs. 12A–F). Quantitative analysis revealed that the promoting effect of TLR9 agonist on maturation was dose-dependent. The proportion of insulin-positive cells (62.5 ± 5.2)% and the proportion of double-positive cells (58.3 ± 4.8%) in the high-dose group (50 mg/kg) were significantly higher than those in the low-dose group (25 mg/kg), which were (40.1 ± 4.5)% and (36.7 ± 4.2)% respectively, $P < 0.01$, Fig. 12G. At the same time, the fluorescence intensity of hormones and the co-localization coefficient in the high-dose group were also significantly higher (all $P < 0.05$, Figs. 12H, I).

## DISCUSSION

Diabetes mellitus (DM) poses a major health burden facing the 21st century with increasing prevalence (Ramu *et al*., 2023; Wang *et al*., 2023), characterized by multiple organs complication that accounts for the primary disability and mortality, further therapies using exogenous insulin impose a heavy burden on patients' lives (Li *et al*., 2023; Xiong *et al*., 2021; Alkhalidi, 2023). Recently, stem cell-derived IPCs have been desired to address this unmet clinical need. Studies (Al-Otaibi *et al*., 2022) have shown that BMSCs can also be used to promote bone repair in fracture rats and exhibit certain effects in diabetic nephropathy and diabetic retinopathy, owing to their multilineage differentiation potential.

BMSCs were obtained from rat bone marrow and identified by flow cytometry, while multidirectional differentiation assay further confirmed that BMSCs cells from rat bone marrow had good differentiation potential. TLR9 agonists were used for further treatment after inducing IPCs differentiation. The results confirmed that TLR9 agonists can effectively promote the maturation of IPC cells after differentiation and significantly upregulate the expression levels of pancreatic endocrine-related genes. BMSC cell transplantation was performed mostly via intrahepatic injection, but most of the transplanted BMSC cells were lost due to an immediate blood-mediated inflammatory response (Feng *et al*., 2025; Yao *et al*., 2023). Current researchers have attempted islet transplantation at other sites, including the omentum pouch, preperitoneal space, abdominal cavity, muscle and caudal vein injection (Barachini *et al*., 2023; Nakafusa *et al*., 2022). However, regardless of the transplantation mode, it can lead to the activation of invasive procedures, thereby reducing the transplantation efficiency. In addition, directional differentiation of BMSCs also significantly affects therapeutic efficacy after transplantation (Han *et al*., 2025; Hazrati *et al*., 2022). Therefore, in this study, differentiated BMSCs were transplanted via TheraCyteTM capsules for packaging, then transplanted into diabetic model rats and treated continuously with TLR9 agonists after transplantation. We found that the use of TLR9 agonists can promote the maturation of BMSCs *in vivo*, thus effectively reducing blood glucose and promoting insulin and C-peptide expression in rats. It should be noted that the dose of the TLR9 agonist used in this study was significantly higher than that reported in most immunomodulation studies (Cascini *et al*., 2023). This is because this study did not precisely regulate systemic immune responses but instead strongly activated the TLR9 signaling pathway to promote IPC differentiation and maturation. Moreover, the TheraCyte capsule may have limited the local effective concentration of the TLR9 agonist, so the TLR9 agonist dose was set higher.

The *in vitro experiments in this study demonstrated that the TLR9 agonist significantly upregulated the expression of core transcription factors, including* PDX1 and NeuroD1, as well as the INS insulin gene, in pancreatic endocrine development in a dose-dependent manner. It also enhanced the insulin and C-peptide secretion capacity. However, this study has not yet verified the expression and nuclear translocation of these transcription factors at the protein level. Future experiments using protein immunoblotting and immunocytochemistry are needed to confirm these findings. In the STZ-induced diabetic rat model, the TLR9 agonist combined with BMSC transplantation significantly improved short-term blood glucose control, accompanied by a synchronous increase in serum insulin and C-peptide levels. Histological analysis further confirmed that in the transplanted capsules treated with TLR9 agonist, the number and fluorescence intensity of insulin and C-peptide double-positive cells significantly increased. Therefore, the TLR9 agonist promoted the development of BMSC-derived IPCs toward mature and functional endocrine cells through activating key transcription programs, enhancing hormone synthesis and secretion and supporting the functional maintenance of transplanted cells *in vivo*.

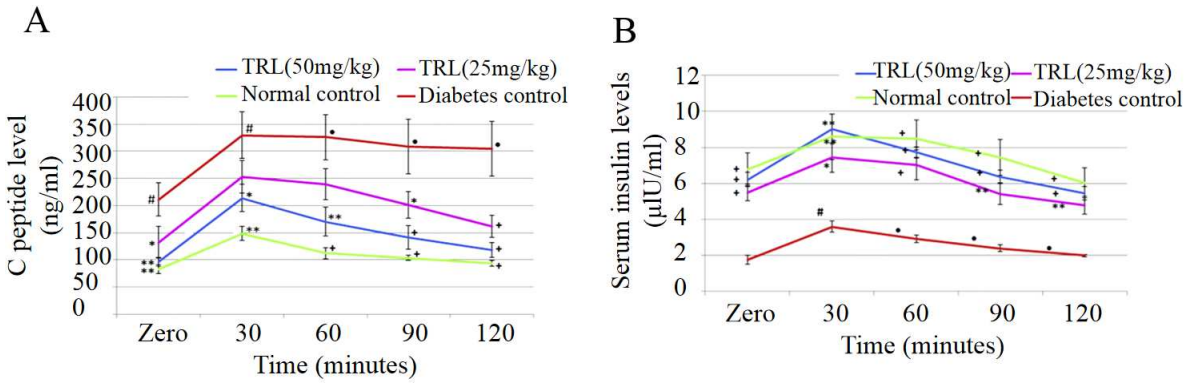


**Fig. 11**: Glucose tolerance test in four groups of rats.
Blood glucose level in four groups of rats in oral glucose tolerance test. (B) Serum insulin level in four groups of rats in oral glucose tolerance test, * P<0.05,**P<0.01,+P<0.001, relative to diabetes group. # P <0.05, ●P<0.01 relative to sham control group.
Note: The trends of fasting blood glucose changes in the four groups of rats. Grouping: Diabetes control group (DM Control, n=10), BMSCs transplantation group (BMSCs Only, n=10), BMSCs + TLR9 (25 mg/kg) group (n=10), BMSCs + TLR9 (50 mg/kg) group (n=10).

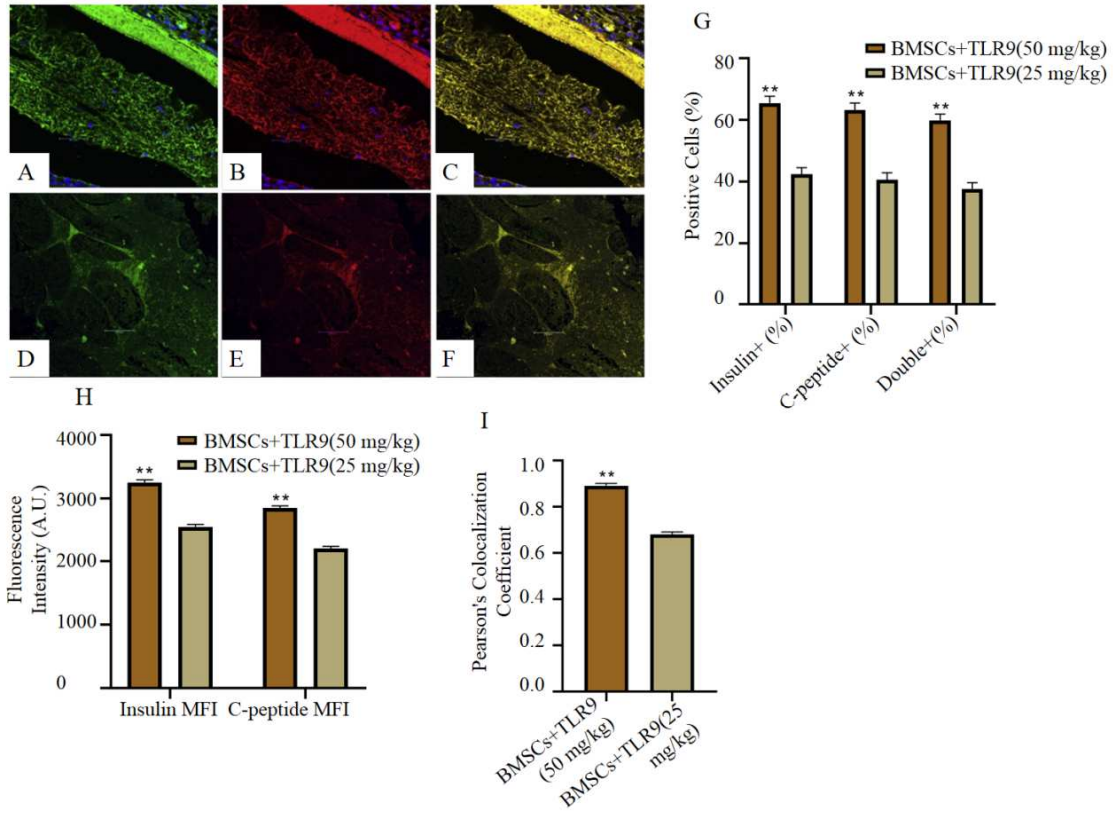


**Fig. 12**: Immunofluorescence analysis of retrieved TheraCyte™ capsules.
Transplant differentiated cells treated by TLR9 agonists (50 mg/kg, A-C) or (25mg/kg, D-F) in rat pancreas. (A or D) Insulin for green, (B or E) c peptide for red, (C or F) colocalization analysis. Original picture x100. (G) Percentage of positive cells: The proportion of insulin-positive (Ins+), C-peptide-positive (C-pep+), and insulin/C-peptide double-positive (Double+) cells among the total number of DAPI+ cell nuclei. (H) Hormone storage level: The average fluorescence intensity of insulin and C-peptide signals within the positive cells (background-subtracted). (I) Subcellular co-localization analysis: The Pearson correlation coefficient between insulin and C-peptide signals. ** P < 0.01 vs the BMSCs + TLR9 (25 mg/kg) group.
Note: Each group had n = 5 animals, and at least 3 non-overlapping fields were analyzed for each animal.

Although this study could not completely rule out the possibility that the transplanted cells exert therapeutic effects through paracrine signals, the cells directly recovered from the capsules showed strong co-expression of insulin and C-peptide, confirming that the BMSC-IPCs treated with a TLR9 agonist successfully differentiated into cells with hormone-synthesizing capabilities in *vivo*. If the efficacy mainly results from paracrine induction, these cells should mainly exhibit secretory phenotypes. Moreover, the changes in blood glucose and insulin levels observed in this study require continuous insulin entry into the systemic circulation. The insulin released locally by the capsules will be diluted before entering the systemic circulation, making it difficult to induce distant host cells to produce large amounts of insulin. Although paracrine effects may exist, the current data support the view that the direct endocrine function of BMSC-IPCs is the main mechanism underlying therapeutic effects. Future studies could use capsules containing only conditioned medium as controls to analyze this further.

Related studies have shown that TLR9 can trigger pyroptosis by activating the NF-κB-NLRP3 axis (Lu *et al*., 2023). However, the function of NF-κB transcription factors depends on their subunits. Previous studies have reported that the p65: p50 heterodimer drives the expression of pro-inflammatory genes, whereas the cRel: p50 heterodimer inhibits the expression of inflammatory molecules (Kaya *et al*., 2025). Therefore, in this study, the activation of TLR9 may promote the formation of inhibitory complexes, such as p50 homodimers, through NF-κB activation, or activate pathways, such as RelB/p52, closely related to cell survival, differentiation and metabolic regulation, thereby promoting the maturation of IPCs. Furthermore, previous studies have indicated that TLR9 can also induce the expression of type I interferons through the IRF7 pathway, subsequently activating the JAK-STAT signaling pathway (Wiest *et al*., 2023; Shemesh *et al*., 2021), which initiates interferon-stimulated genes (Han *et al*., 2023), which may directly support insulin synthesis and secretion by enhancing cellular metabolism, endoplasmic reticulum function and stress resistance. Additionally, TLR9 may synergistically activate MAPK and other signaling pathways through the MyD88-dependent pathway (Kochumon *et al*., 2022), upregulate key pancreatic development transcription factors such as PDX1 and NeuroD1 and ultimately promote the transcriptional activation of insulin-related genes.

This study confirmed that TLR9 agonists significantly promote the functional maturation of BMSC-IPCs. However, the underlying molecular mechanism requires further verification using TLR9-specific inhibitors, siRNA gene silencing, or blocking experiments targeting key pathway molecules in the future. Nevertheless, this study has confirmed the positive role of TLR9 agonists in the differentiation of BMSC-IPCs, providing important preliminary experimental evidence for subsequent mechanism research.

Furthermore, TLR9 agonists can dose-dependently promote the differentiation of BMSCs into IPCs and upregulate the expression of key β-cell genes *in vitro*; in diabetic rat models, they can significantly lower blood glucose and increase insulin levels. However, all metabolic improvements are rapidly reversed after drug withdrawal, indicating that this effect results from continuous pharmacological stimulation of the transplanted cells by the agonist rather than from stable cell reprogramming. Therefore, this study has established a novel "stem cell-immune modulator" synergistic treatment strategy, providing a potential short-term intensification plan for diabetes.

Converting this effective short-term stimulation into autonomous, persistent cell function in transplanted cells is a challenge for achieving breakthrough treatment. It should be noted that the verification of the functional maturity of IPCs in this study mainly relies on the expression and co-localization of insulin and C-peptide. Although this is a necessary condition for functional differentiation, confirming that they have differentiated into mature β-like cells with glucose-sensing and secretion functions requires additional evidence. Therefore, the cells generated in this study should be more accurately defined as IPCs with insulin-synthesizing capacity or β-cell precursors. Their exact maturity stage and complete functional characteristics need to be systematically evaluated in subsequent studies.

## CONCLUSION

In conclusion, TLR9 agonists can serve as an effective adjunct, dose-dependently enhancing the short-term secretion function of transplanted BMSC-derived IPCs, thereby achieving significant but reversible improvement in blood glucose levels in diabetic rat models. This effect is associated with enhanced insulin/C-peptide synthesis and secretion capacity in cells. However, this study has certain limitations. For instance, this study is preclinical basic research, and its results cannot be directly extrapolated to clinical applications.; the assessment of cell functional maturity and the long-term status of the transplantation system is insufficient; the safety of high-dose TLR9 agonists has not been systematically verified; the stability of the internal reference gene and the efficiency of the primers in the qPCR data have not been verified. In the future, by optimizing the dosage and administration scheme, improving the functional and safety assessment system and using lineage-tracing and other mechanistic research tools, it is necessary to establish a group using only TLR9 agonists and a sham surgery control group implanted with empty capsules to further explore in depth.

***Acknowledgments***
This work was supported by the National Science Foundation of China (NSFC) (No. 82172389).

***Authors' contributions***
Chuan Liu: Conceptualization, Methodology, Investigation, Formal analysis, Writing – Original Draft; Huayong Zheng: Methodology, Investigation, Data Curation; Peng Lu: Methodology, Resources, Investigation; Jing Tian: Resources, Validation; Yenuan Hu: Resources, Project administration; Li Yao: Supervision, Funding acquisition, Writing – Review & Editing; Tiansheng Sun: Conceptualization, Supervision, Funding acquisition, Writing – Review & Editing, Project administration.
All authors have read and agreed to the published version of the manuscript.

***Funding***
There was no funding.

***Data availability statement***
All data generated or analysed during this study are included in this published article [and its supplementary information files]. [Only use this if all data is in the manuscript or supplementary files.

***Ethical approval***
This study was approved by the ethics committee of The Forth Medical Center of Chinese PLA General Hospital (Approval Number: 82172389). All animal experiments in this study were conducted in accordance with the "Regulations on the Administration of Laboratory Animals" of China and relevant international guidelines. Throughout the entire research process, the approved protocol was strictly followed to ensure that the animals received adequate food, water and an appropriate living environment. All invasive procedures were performed under appropriate anesthesia and analgesia and clear humane endpoints were established to alleviate the potential pain the animals might experience. This study was performed in adherence with the ARRIVE guidelines. See supplementary file for the ARRIVE checklist.

***Conflict of interest***
The authors declare no conflict of interest.

***Supplementary data***
https://www.pjps.pk/uploads/2026/05/SUP1778833999.pdf

## REFERENCES

Alkhalidi F (2023). A comparative study to assess the use of chromium in type 2 diabetes mellitus. *J Med Life*., **16**(8): 1178–1182.

Al-Otaibi AM, Al-Gebaly AS, Almeer R, Albasher G, Al-Qahtani WS and Abdel Moneim AE (2022). Melatonin pre-treated bone marrow derived-mesenchymal stem cells prompt wound healing in rat models. *Biomed Pharmacother*., **145**: 112473.

Barachini S, Biso L, Kolachalam S, Petrini I, Maggio R, Scarselli M and Longoni B (2023). Mesenchymal stem cell in pancreatic islet transplantation. *Biomedicines*., **11**(5): 1426.

Bjornstad P, Drews KL, Caprio S, Gubitosi-Klug R, Nathan DM, Tesfaldet B, Tryggestad J, White NH and Zeitler P (2021). Long-term complications in youth-onset type 2 diabetes. *N Engl J Med.,* **385**(5): 416-426.

Cascini C, Ratti C, Botti L, Parma B, Cancila V, Salvaggio A, Meazza C, Tripodo C, Colombo MP and Chiodoni C (2023). Rewiring innate and adaptive immunity with TLR9 agonist to treat osteosarcoma. *J Exp Clin Cancer Res*., **42**(1): 154.

Chan JCH and Chan MCY (2022). Novel drugs for diabetes also have dramatic benefits on hard outcomes of heart and kidney disease. *Curr Cardiol Rev*., **18**(6): e110522204572.

Dai L and Wang Q (2025). Two-pronged approach: Therapeutic effect of biological scaffold combined with immune intervention and β-cell replacement on type 1 diabetic mice. *Diabetes Obes Metab*., **27**(6): 3464–3476.

Dilworth L, Stennett D, Facey A, Omoruyi F, Mohansingh S and Omoruyi FO (2024). Diabetes and the associated complications: The role of antioxidants in diabetes therapy and care. *Biomed Pharmacother*., **181**: 117641.

Duan W, Zou H, Zang N, Ma D, Yang B and Zhu L (2023). Metformin increases bone marrow adipose tissue by promoting mesenchymal stromal cells apoptosis. *Aging (Albany NY)*., **15**(2): 542-552.

Ebrahim N, El-Halim HEA, Helal OK, El-Azab NE, Badr OAM, Hassouna A, Saihati HAA, Aborayah NH, Emam HT, El-Wakeel HS, Aljasir M, El-Sherbiny M, Sarg NAS, Shaker GA, Mostafa O, Sabry D, Fouly MAK, Forsyth NR, Elsherbiny NM and Salim RF (2022). Effect of bone marrow mesenchymal stem cells-derived exosomes on diabetes-induced retinal injury: Implication of Wnt/ b-catenin signaling pathway. *Biomed Pharmacother*., **154**: 113554.

Feng X, Feng B, Zhou J, Yang J, Pan Q, Yu J, Shang D, Li L and Cao H (2025). Mesenchymal stem cells alleviate mouse liver fibrosis by inhibiting pathogenic function of intrahepatic B cells. *Hepatology*., **81**(4): 1211–1227.

Han J, Zheng Q, Cheng Y, Liu Y, Bai Y, Yan B, Guo S, Yu J, Li X and Wang C (2022). Toll-like receptor 9 (TLR9) gene deletion-mediated fracture healing in type II diabetic osteoporosis associates with inhibition of the nuclear factor-kappa B (NF-κB) signaling pathway. *Bioengineered*., **13**(5): 13689–13702.

Han J, Wu M and Liu Z (2023). Dysregulation in IFN-γ signaling and response: The barricade to tumor immunotherapy. *Front Immunol*., **14**: 1190333.

Han X, Liao R, Li X, Zhang C, Huo S, Qin L, Xiong Y, He T, Xiao G and Zhang T (2025). Mesenchymal stem cells

in treating human diseases: Molecular mechanisms and clinical studies. *Signal Transduct Target Ther*., **10**(1): 262.

Hazrati A, Malekpour K, Soudi S and Hashemi SM (2022). Mesenchymal stromal/stem cells spheroid culture effect on the therapeutic efficacy of these cells and their exosomes: A new strategy to overcome cell therapy limitations. *Biomed Pharmacother*., **152**: 113211.

Kaya Z, Belder N, Sever-Bahcekapili M, Erdener ŞE, Donmez-Demir B, Bagcı C, Koroglu MN, Bilguvar K and Dalkara T (2025). Spreading depolarization triggers pro- and anti-inflammatory signalling: A potential link to headache. *Brain*., **148**(7): 2522–2536.

Khokhani P, Warmink K, Kruyt M, Weinans H and Gawlitta D (2025). Mixtures of PRR ligands partly mimic the immunomodulatory response of γi staphylococcus aureus, enhancing osteogenic differentiation of human mesenchymal stromal cells. *Stem Cells Int*., **2025**: 1445520.

Kochumon S, Arefanian H, Sindhu S, Thomas R, Jacob T, Al-Sayyar A, Shenouda S, Al-Rashed F, Koistinen HA, Al-Mulla F, Tuomilehto J and Ahmad R (2022). Expression of steroid receptor RNA activator 1 (SRA1) in the adipose tissue is associated with TLRs and IRFs in diabesity. *Cells*., **11**(24): 4007.

Li B, Li W, Liu T and Zha L (2023). Extracellular vesicles regulate the transmission of insulin resistance and redefine noncommunicable diseases. *Front Mol Biosci*., **9**: 1024786.

Li W, Jin L, Cui Y, Nie A, Xie N and Liang G (2021). Bone marrow mesenchymal stem cells-induced exosomal microRNA-486-3p protects against diabetic retinopathy through TLR4/NF-κB axis repression. *J Endocrinol Invest*., **44**(6): 1193–1207.

Lu P, Zheng H, Meng H, Liu C, Duan L, Zhang J, Zhang Z, Gao J, Zhang Y and Sun T (2023). Mitochondrial DNA induces nucleus pulposus cell pyroptosis via the TLR9-NF-κB-NLRP3 axis. *J Transl Med*., **21**(1): 389.

Luo W, Geng Y, Gao M, Cao M, Wang J, Yang J, Sun C and Yan X (2022). Isolation and identification of bone marrow mesenchymal stem cells from forest musk deer. *Animals (Basel)*., **13**(1): 17.

Mori T, Yamamoto Y, Hanai K, Yamashige Y, Murata H, Shinozaki T and Nakagami T (2026). Remnant cholesterol and kidney disease progression in type 2 diabetes: A retrospective cohort study. *J Clin Lipidol*., **20**(1): 135–144.

Nakafusa Y, Nitta N, Ishii K, Shirasu N, Iwamoto T, Nemoto T, Nakamura M, Goto M, Iwata H, Taniguchi M and Yasunami Y (2022). Acceptance of murine isl*et al*lografts without immunosuppression in inguinal subcutaneous white adipose tissue pretreated with bFGF. *Diabetes*., **71**(8): 1721–1734.

Ramu D, Ramaswamy S, Rao S and Paul SFD (2023). The worldwide prevalence of latent autoimmune diabetes of adults among adult-onset diabetic individuals: A systematic review and meta-analysis. *Endocrine*., **82**(1): 28–41.

Russo MP, Grande-Ratti MF, Burgos MA, Molaro AA and Bonella MB (2023). Prevalence of diabetes, epidemiological characteristics and vascular complications. Prevalencia de diabetes, caracteristicas epidemiologicas y complicaciones vasculares. *Arch Cardiol Mex*., **93**(1): 30–36.

Saccu G, Menchise V, Gai C, Bertolin M, Ferrari S, Giordano C, Manco M, Dastrù W, Tolosano E, Bussolati B, Calautti E, Camussi G, Altruda F and Fagoonee S (2022). Bone marrow mesenchymal stromal/stem cell-derived extracellular vesicles promote corneal wound repair by regulating inflammation and angiogenesis. *Cells*., **11**(23): 3892.

Shao Y, Sun L, Ma B, Jin R, Ban Y, Li R, Wang J, Lian H and Yue H (2023). VCAM-1 promotes angiogenesis of bone marrow mesenchymal stem cells derived from patients with trauma-induced osteonecrosis of the femoral head by regulating the apelin/CCN2 pathway. *Stem Cells Int*., **2023**: 6684617.

Shemesh M, Lochte S, Piehler J and Schreiber G (2021). IFNAR1 and IFNAR2 play distinct roles in initiating type I interferon-induced JAK-STAT signaling and activating STATs. *Sci Signal*., **14**(710): eabe4627.

TODAY Study Group, Bjornstad P, Drews KL, Caprio S, Gubitosi-Klug R, Nathan DM, Tesfaldet B, Tryggestad J, White NH and Zeitler P (2021). Long-term complications in youth-onset type 2 diabetes. *N Engl J Med*., **385**(5): 416–426.

Utami A, Putra A, Wibowo JW, Amalina ND and Satria Irawan RC (2023). Hypoxic secretome mesenchymal stem cells inhibiting interleukin-6 expression prevent oxidative stress in type 1 diabetes mellitus. *Med Glas (Zenica)*., **20**(2): 10.17392/1538-23.

Wang Z, Wu C, Yin D and Dou K (2025). Ferroptosis: Mechanism and role in diabetes-related cardiovascular diseases. *Cardiovasc Diabetol*., **24**(1): 60.

Wang M, Li Y, Li S and Lv J (2022). Endothelial dysfunction and diabetic cardiomyopathy. *Front Endocrinol (Lausanne)*., **13**: 851941.

Wang Y, Li W, Guo Y, Huang Y, Guo Y, Song J, Mei F, Liao P, Gong Z, Chi X and Deng X (2024). Mitochondria transplantation to bone marrow stromal cells promotes angiogenesis during bone repair. *Adv Sci (Weinh)*., **11**(39): e2403201.

Wang J, Dai P, Zou T, Lv Y, Zhao W, Zhang X and Zhang Y (2021). Transcriptome analysis of the transdifferentiation of canine BMSCs into insulin producing cells. *BMC Genomics*., **22**(1): 134.

Wang W, Ji Q, Ran X, Li C, Kuang H, Yu X, Fang H, Yang J, Liu J, Xue Y, Feng B, Lei M and Zhu D (2023). Prevalence and risk factors of diabetic peripheral neuropathy: A population-based cross-sectional study in

China. *Diabetes Metab Res Rev*., **39**(8): e3702.

Waris S, Begam HH, Kumar MP, Abdulrasool ZHI, Avudaiappan M, Butler AE and Nandakumar M (2026). Stem cell-derived beta-cell therapies: Encapsulation advances and immunological hurdles in diabetes treatment. *Cells*, **15**(2): 191.

Wen WX, Cao Y, Chen P, Li JH, Li WW, Huang GL, Zheng HX, Zhu XL, Zhang H, Chen YX, Huang XH, Hu YZ and Huang YL (2024). A reliable strategy for establishment of an animal model of diabetic cardiomyopathy: Induction by a high-fat diet combined with single or multiple injections of low-dose streptozotocin. *Life Sciences*, **358**: 123161.

Wiest MJ, Gu C, Ham H, Gorvel L, Keddis MT, Griffing LW, Joo H, Gorvel JP, Billadeau DD and Oh S (2023). Disruption of endosomal trafficking with EGA alters TLR9 cytokine response in human plasmacytoid dendritic cells. *Front Immunol*., **14**: 1144127.

Xiong J, Hu H, Guo R, Wang H and Jiang H (2021). Mesenchymal stem cell exosomes as a new strategy for the treatment of diabetes complications. *Front Endocrinol (Lausanne)*., **12**: 646233.

Yao Q, Chen W, Yu Y, Gao F, Zhou J, Wu J, Pan Q, Yang J, Zhou L, Yu J, Cao H and Li L (2023). Human placental mesenchymal stem cells relieve primary sclerosing cholangitis via upregulation of TGR5 in Mdr2-/- mice and human intrahepatic cholangiocyte organoid models. *Research (Wash D C)*., **6**: 0207.

Zhang Y, Luo Y, Han J, Wang L, Xu H, Zhang L, Chen P and Luo H (2026). Bone Marrow Mesenchymal Stem Cell-Derived Exosomal Let-7b-5p Reduces High Glucose-Induced Microglial Activation and Inflammation Through TLR4/ATF4. *Mediators Inflamm*., **2026**: 7251718.